

Comparative Reactive Blue 4 Dye Removal by Lemon Peel Bead Doping with Iron(III) Oxide-Hydroxide and Zinc Oxide

Pornsawai Praipipat,* Pimploy Ngamsurach, and Vatcharaporn Prasongdee

Cite This: *ACS Omega* 2022, 7, 41744–41758

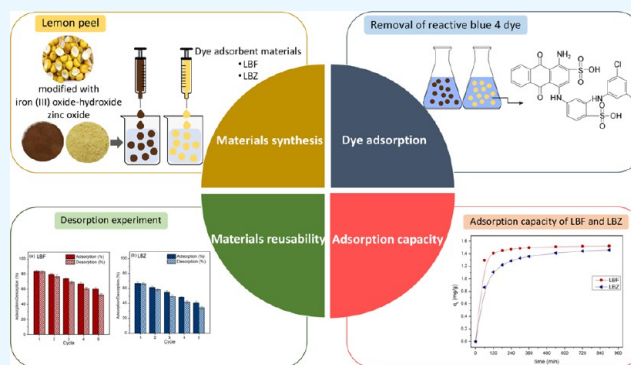
Read Online

ACCESS |

Metrics & More

Article Recommendations

ABSTRACT: The increasing concern of dye contamination in wastewater results in the toxicity of aquatic life and water quality, so wastewater treatment is required to treat the low water quality standard for safety purposes. Lemon peel beads-doped iron(III) oxide-hydroxide (LBF) and lemon peel beads-doped zinc oxide (LBZ) were synthesized and characterized to investigate their crystalline structure, surface morphology, chemical compositions, chemical functional groups, and ζ potentials by X-ray diffraction, field emission scanning electron microscopy and focused ion beam, energy dispersive X-ray spectroscopy, Fourier transform infrared, and zetasizer techniques. Their effects of dose, contact time, temperature, pH, and concentration for reactive blue 4 (RB4) dye removal efficiencies were investigated by batch experiments, and their adsorption isotherms, kinetics, and desorption experiments were also studied. LBF and LBZ demonstrated semicrystalline structures, and their surface morphologies had a spherical shape with coarse surfaces. Five main elements of carbon (C), oxygen (O), calcium (Ca), chlorine (Cl), and sodium (Na) and six main function groups of O–H, C≡N, C=C, C–OH, C–O–C, and C–H were detected in both materials. The results of ζ potential demonstrated that both LBF and LBZ had negative charges on the surface at all pH values, and their surfaces increased more of the negative charge with the addition of the pH value from 2–12. For batch tests, the RB4 dye removal efficiencies of LBF and LBZ were 83.55 and 66.64%, respectively, so LBF demonstrated a higher RB4 dye removal efficiency than LBZ. As a result, the addition of iron(III) oxide-hydroxide helped in improving the material efficiency more than zinc oxide. In addition, both LBF and LBZ could be reused in more than five cycles for RB4 dye removal of more than 41%. The Freundlich model was a good explanation for their adsorption patterns relating to physiochemical adsorption, and a pseudo-second-order kinetic model was a well-fitted model for explaining their adsorption mechanism correlating to the chemisorption process with heterogeneous adsorption. Therefore, LBF was a potential adsorbent to further apply for RB4 dye removal in industrial applications.



1. INTRODUCTION

Since dyes have been widely used in many industrial processes of textiles, paint, and pigments, the dye contaminated in wastewater is a concern because of its non-biodegradation and toxicity.¹ Dye contaminated in receiving water can be an obstacle to the transmission of sunlight for plant photosynthesis as well as toxic to aquatic organisms, resulting in increased bioaccumulation through the food chain.² Although various dyes are used in many industries, such as basic dyes, direct dyes, acid dyes, and azoic dyes, depending upon their objectives, reactive dyes are popularly used for dyeing cellulose fibers because of their long-lasting color. However, it is a stable polyaromatic molecule, so it has a difficult natural biodegradation process.³ As a result, the wastewater treatment of contaminated dye is required before discharging it to the water body for a safe environment.

Many conventional methods of coagulation–flocculation, chemical precipitation, advanced oxidation processes, ion

exchange, photocatalytic degradation, and adsorption are applied for dye removal;⁴ however, the weighing of the advantage–disadvantage, operation method, and budget is used as the main consideration to choose the wastewater treatment system. Since adsorption is an effective method with easy operation, reasonable cost, and several available adsorbents, this method is popularly used. To save operating costs, a low-cost adsorbent is an interesting option, so wastes from agriculture, industries, and food such as bagasse, sawdust, rice husk, coconut shells, peach gum, banana peels, and lemon

Received: September 14, 2022

Accepted: October 24, 2022

Published: November 1, 2022



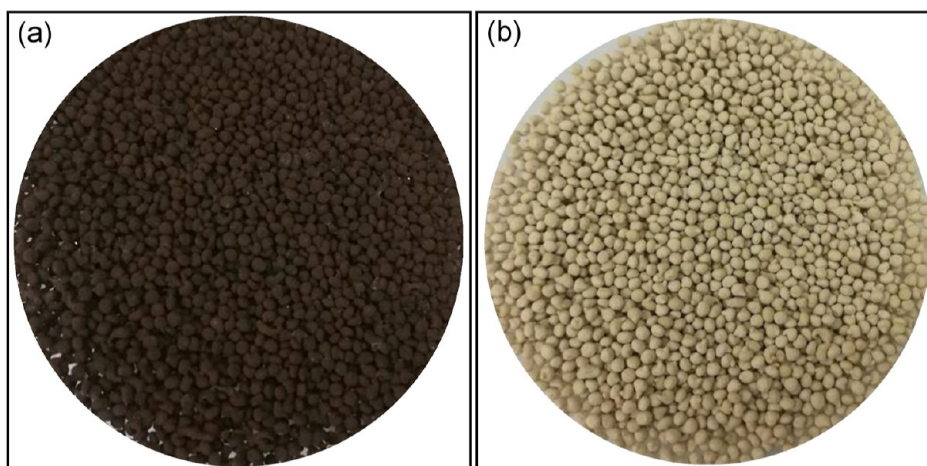


Figure 1. Physical characteristics of (a) LBF and (b) LBZ.

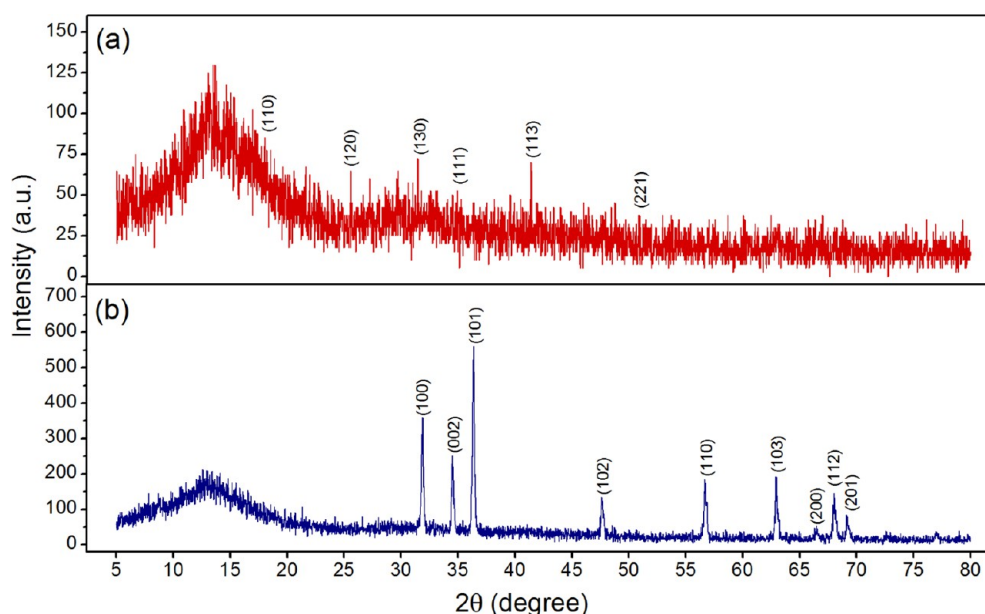


Figure 2. Crystalline structures of (a) LBF and (b) LBZ.

peels might be a good option for dye removal with the confirmation of previous studies.^{5–7} Among those, lemon peels are an interesting choice because not only do they have good chemical properties of cellulose, hemicellulose, lignin, and pectin, including carboxyl and hydroxyl groups for dye removal,⁸ but they can also help to reduce a huge amount of food waste such as recycled waste for wastewater treatment as well.

Although the raw materials above are potential materials for dye removal in wastewater, it might be better if they could increase their material efficiencies for high dye removal in the case of high-strength wastewater. As a result, many studies have developed material efficiency by adding several metal oxides like titanium dioxide (TiO_2), aluminum oxide (Al_2O_3), copper oxide (CuO), manganese oxide (MnO), iron(II,III) oxide (Fe_3O_4 or Fe_2O_3), and zinc oxide (ZnO).^{9–11} Among these, Fe_3O_4 or Fe_2O_3 and ZnO are popularly used for improving material efficiencies to remove the dye in many articles.^{12–15} Therefore, this study attempts to synthesize dye-adsorbent materials from lemon peels modified with iron(III) oxide-hydroxide and zinc oxide in a bead form to increase

material efficiency and make it feasible to be an alternative dye adsorbent for an industrial application.

This study aimed to synthesize two dye-adsorbent materials of lemon peel beads-doped iron(III) oxide-hydroxide (LBF) and lemon peel beads-doped zinc oxide (LBZ) for reactive blue 4 (RB4) dye removal in an aqueous solution to identify their crystalline structure, surface morphology, chemical compositions, chemical functional groups, and ζ potentials by X-ray diffraction (XRD), field emission scanning electron microscope and focused ion beam (FESEM–FIB), energy dispersive X-ray spectroscopy (EDX), Fourier transform infrared (FTIR), and zetasizer techniques; to investigate their RB4 dye removal efficiencies with affecting factors of dosage, contact time, temperature, pH, and initial concentration by a series of batch experiments; to study their adsorption patterns and mechanisms by studying adsorption isotherms and kinetics; and to examine desorption experiments.

2. RESULTS AND DISCUSSION

2.1. Physical Characteristics of LBF and LBZ. The physical characteristics of LBF and LBZ are demonstrated in

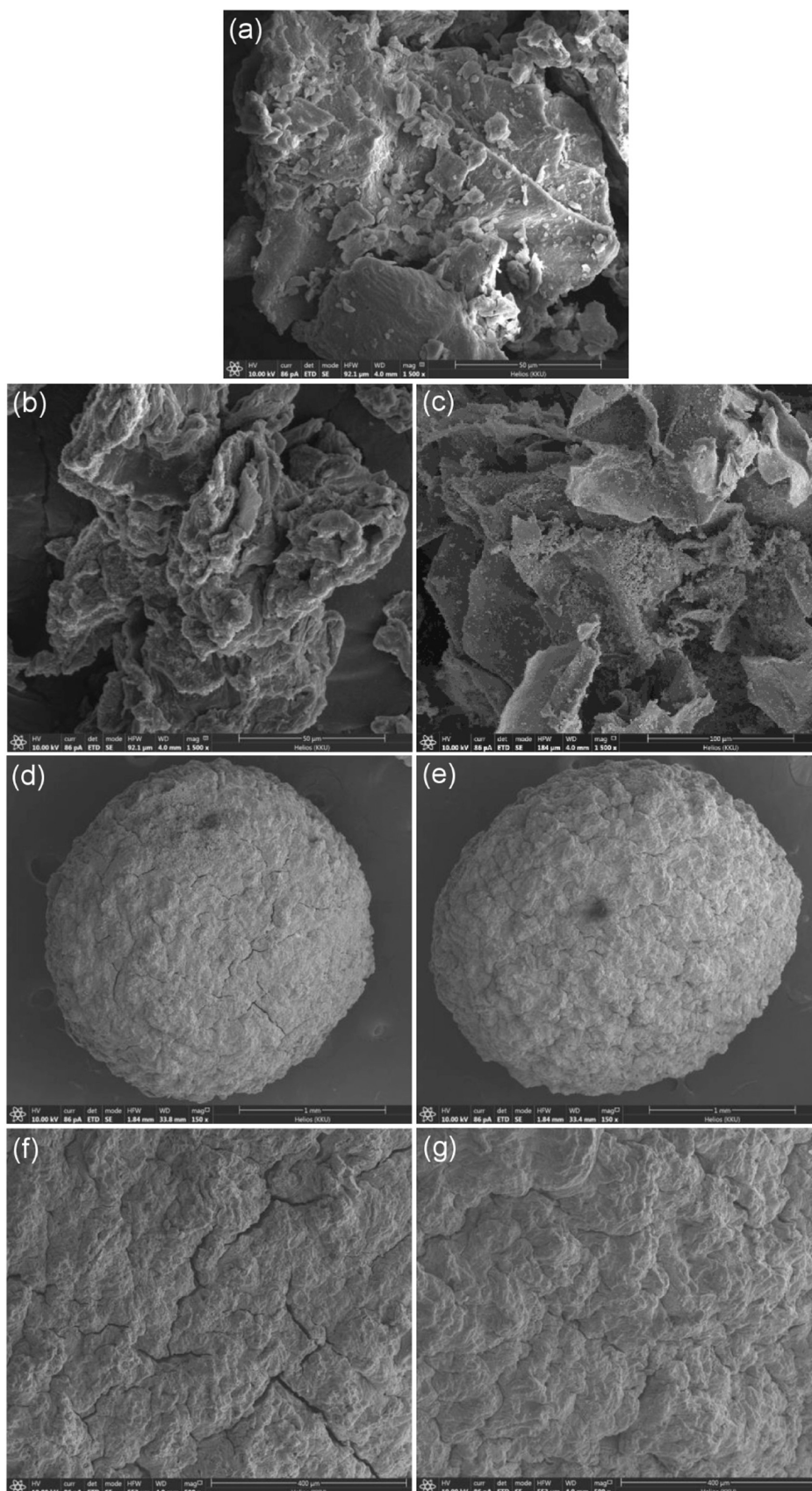


Figure 3. FESEM–FIB images of surface morphologies of (a) LP, (b) LPF, and (c) LPZ with 1500× magnification with 50 or 100 μm and (d,f) LBF and (e,g) LBZ at 150× magnification with 1 mm for the bead form and at 500× magnification with 400 μm for the surface, respectively.

Figure 1a,b which depicted a spherical shape with different colors depending on the types of metal oxides inside the materials. LBF was an iron-rust beaded color matched to the color of iron(III) oxide-hydroxide shown in Figure 1a, whereas LBZ was a light-yellow beaded color from the decreasing yellow color of lemon peels by the white color of zinc oxide shown in Figure 1b. Therefore, the type of metal oxide is highly affected by the changing color of bead materials.

2.2. Characterizations of LBF and LBZ. **2.2.1. X-ray Diffraction.** Crystalline structures of LBF and LBZ by XRD analysis are demonstrated in Figure 2a,b which displayed the semicrystalline structures. LBF demonstrated semicrystalline structures with specific peaks of sodium alginate and iron(III) oxide-hydroxide. The specific peaks of sodium alginate were detected at 2θ of 13.50, 18.20, 20.20, 21.58, 24.44, 28.56, and 38.16°¹⁶ and 2θ of 21.66, 26.66, 33.20, 36.30, 41.40, and 53.54°, which were found to be specific peaks of iron(III) oxide-hydroxide matched to JCPDS: 29-0713¹⁷ shown in Figure 2a. For LBZ, the specific peaks of sodium alginate were similarly detected to LBF, and the 2θ of 31.88, 34.54, 36.38, 47.64, 56.68, 62.94, 66.32, 68.02, and 69.10° related to JCPDS: 36-1451¹⁸ was identified as the specific peaks of zinc oxide shown in Figure 2b.

2.2.2. FESEM-FIB and EDX. The surface morphologies of lemon peel powder (LP), lemon peel powder-doped iron(III) oxide-hydroxide (LPF), lemon peel powder-doped zinc oxide (LPZ), LBF, and LBZ were analyzed by FESEM-FIB analysis. Figure 3a–c illustrated the surface morphologies of LP, LPF, and LPZ and that they were uneven surfaces at 1500X magnification with 50 or 100 μm , which LP demonstrated a smoother surface than LPF and LPZ. In Figure 3d,e, they presented LBF and LBZ in a whole bead at 150X magnification with 1 mm, which had a spherical shape with coarse surfaces. In addition, their surfaces were heterogeneous, with rough surfaces zoomed at 500X magnification with 400 μm shown in Figure 3f,g.

EDX analysis was used to identify the chemical compositions of LBF and LBZ, and the results are demonstrated in Table 1. Five main elements of carbon (C), oxygen (O),

Table 1. Chemical Compositions of LBF and LBZ by EDX Analysis

materials	chemical element (wt %)						
	C	O	Ca	Cl	Na	Fe	Zn
LBF	36.7	32.0	7.0	3.2	2.7	18.4	
LBZ	34.5	25.2	5.5	2.9	3.1		28.8

calcium (Ca), chlorine (Cl), and sodium (Na) were detected in both materials, whereas iron (Fe) and zinc (Zn) were found only in dye materials modified with iron(III) oxide-hydroxide and zinc oxide. For LBF, the percentages by weight (wt %) of C, O, Ca, Cl, Na, Fe, and Zn were 36.7, 32.0, 7.0, 3.2, 2.7, 18.4, and 0%, respectively. For LBZ, the percentages by weight (wt %) of C, O, Ca, Cl, Na, Fe, and Zn were 34.5, 25.2, 5.5, 2.9, 3.1, 0, and 28.8%, respectively. As a result, the results could be proved by the successful addition of iron(III) oxide-hydroxide and zinc oxide into LBF and LBZ.

2.2.3. Fourier Transform Infrared. The chemical functional groups of LBF and LBZ by FTIR analysis were illustrated in Figure 4a,b which had six main functional groups of O–H, C≡N, C=C, C–OH, C–O–C, and C–H. For O–H and C≡N, they represented the carboxylic acids of cellulose,

hemicellulose, lignin, and pectin bonding and nitrile link.¹⁹ C=C demonstrated an aromatic ring of lignin and C–OH, illustrating the carbonate ions of lemon peels.²⁰ Finally, C–O–C identified sodium alginate of glucosidal linkages, and C–H presented aromatic rings and fibers of lemon peels.²¹ For LBF, it detected O–H at 3727.84 and 3283.05 cm^{-1} , C≡N at 2349.71 cm^{-1} , C=C at 1594.02 cm^{-1} , C–OH at 1414.09 cm^{-1} , C–O–C at 1009.26 cm^{-1} , and C–H at 875.49 cm^{-1} shown in Figure 4a. For LBZ, it detected O–H at 3728.18 and 3286.27 cm^{-1} , C≡N at 2349.80 and 2327.76 cm^{-1} , C=C at 1597.82 cm^{-1} , C–OH at 1417.85 cm^{-1} , C–O–C at 1007.46 cm^{-1} , and C–H at 823.57 cm^{-1} shown in Figure 4b.

2.2.4. ζ Potential. The ζ potentials of LBF and LBZ were investigated using a Zetasizer Nano under different pH values from 2 to 12, and the results are illustrated in Figure 5. The ζ potential values of LBF and LBZ were approximately in the ranges of –3.0 to –31.2 and –5.5 to 37.4 mV, respectively. The surface charges of both materials demonstrated more negative charges with the increase in pH values from 2 to 12, which might result from the increase of hydroxyl ions (OH^-) on their surfaces.²² However, LBZ demonstrated more negative charges on the surface than LBF did in all pH values, which possibly meant that LBF could be caught up, with the RB4 dye ions being more than LBZ because of low-competition anionic ions on the surface.

2.3. Batch Experiments. **2.3.1. Effect of Dose.** The doses in the range of 0.5 to 3.0 g of LBF and LBZ with the control condition of the initial RB4 dye concentration of 50 mg/L, a sample volume of 100 mL, a contact time of 12 h, a pH of 7, a temperature of 30 °C, and a shaking speed of 150 rpm were used to investigate the dose effect, and the results are demonstrated in Figure 6a. RB4 dye removal efficiencies of LBF and LBZ were increased with the increase in material dosage, and 3 g demonstrated the highest RB4 dye removal efficiencies in both materials at 82.97 and 66.76% for LBF and LBZ. Therefore, 3 g was used as the optimum dosage of LBF and LBZ for a contact time effect.

2.3.2. Effect of Contact Time. The contact time from 3 to 18 h of LBF and LBZ with the control conditions of the optimum dosage from 2.3.1, the initial RB4 dye concentration of 50 mg/L, a sample volume of 100 mL, a pH of 7, a temperature of 30 °C, and a shaking speed of 150 rpm were used to study the contact time effect, and the results are presented in Figure 6b. RB4 dye removal efficiencies of LBF and LBZ were increased with the increase in contact time, and 6 and 9 h demonstrated the highest RB4 dye removal efficiencies at 85.39 and 67.89% for LBF and LBZ, respectively. Therefore, those contact times were the optimum contact times of both materials and were used for a temperature effect.

2.3.3. Effect of Temperature. The temperature ranging from 30 to 80 °C of LBF and LBZ with the control conditions of the optimum dosage, contact time from 2.3.1 to 2.3.2, the initial RB4 dye concentration of 50 mg/L, a sample volume of 100 mL, a pH of 7, and a shaking speed of 150 rpm were used to examine the temperature effect, and the results are shown in Figure 6c. RB4 dye removal efficiencies of LBF and LBZ decreased with the increase in temperature, and 30 °C demonstrated the highest RB4 dye removal efficiencies of 83.77 and 66.47% for LBF and LBZ, respectively. Therefore, 30 °C was used as the optimum temperature of LBF and LBZ for a pH effect.

2.3.4. Effect of pH. The pH values of 3–11 of LBF and LBZ with the control conditions of the optimum dosage, contact

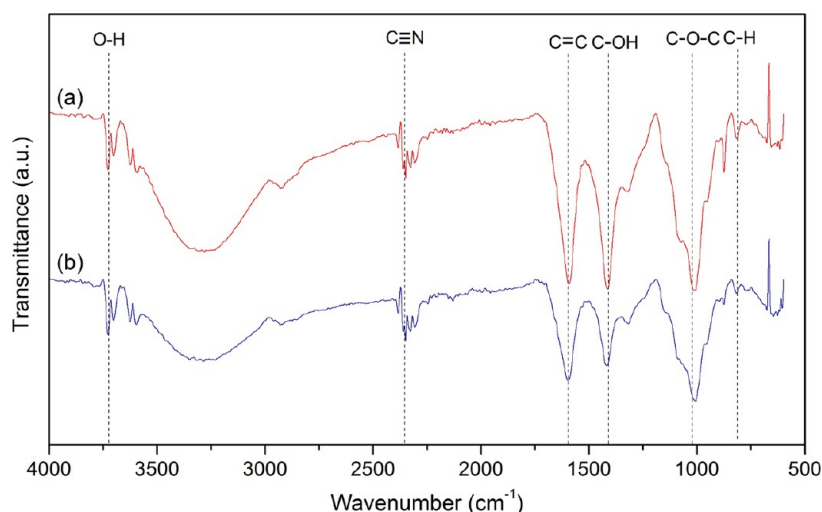


Figure 4. FTIR spectra of (a) LBF and (b) LBZ.

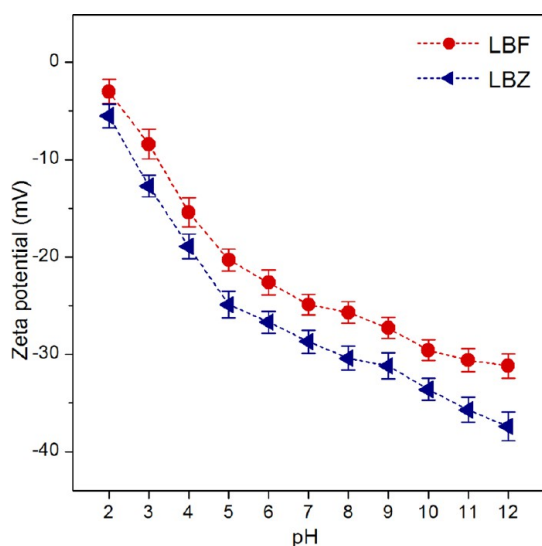


Figure 5. ζ potentials of LBF and LBZ under different pH values.

time, temperature from 2.3.1 to 2.3.3, the initial RB4 dye concentration of 50 mg/L, a sample volume of 100 mL, and a shaking speed of 150 rpm were used to determine the pH effect, and the results are displayed in Figure 6d. RB4 dye removal efficiencies of LBF and LBZ decreased with the increase in pH values, with pH 3 demonstrating the highest RB4 dye removal efficiencies at 83.14 and 67.08% for LBF and LBZ, respectively. This result also corresponded to the result of ζ potential that pH 3 has a less negative charge on the surface than other pH values, supporting high RB4 dye adsorption. In addition, the pH results agreed with other studies that showed that anionic dyes were highly adsorbed at low pH or acidic pH because of the electrostatic interaction on the positively charged surface of dye-adsorbent materials.²³ In contrast, the increase in pHs, especially alkaline pHs, affects the increase of $-\text{OH}$ or negatively charged sites of dye-adsorbent materials, so dye removal efficiencies were decreased. Therefore, pH 3 was the optimum pH for both materials and was used for a concentration effect.

2.3.5. Effect of Concentration. The concentration ranging from 30 to 90 mg/L of LBF and LBZ with the control conditions of the optimum dosage, contact time, temperature,

pH from 2.3.1 to 2.3.4, a sample volume of 100 mL, and a shaking speed of 150 rpm were used to study the concentration effect, and the results are reported in Figure 6e. RB4 dye removal efficiencies from 30 to 90 mg/L of LBF and LBZ were 72.33–87.15 and 57.25–74.91%, which decreased with the increase in RB4 dye concentration. For the RB4 dye concentration of 50 mg/L, the RB4 dye removal efficiencies of LBF and LBZ were 83.55 and 66.64%, and LBF demonstrated a higher RB4 dye removal efficiency than LBZ.

Finally, 3 g, 6 h, 30 °C, pH 3, and 50 mg/L and 3 g, 9 h, 30 °C, pH 3, and 50 mg/L were, respectively, the optimum conditions for dose, contact time, temperature, pH, and concentration of LBF and LBZ. Therefore, the addition of iron(III) oxide-hydroxide helped us to increase material efficiency for RB4 dye adsorption more than the addition of zinc oxide into the lemon peel because LBF spent less contact time than LBZ. This study corresponded to the previous study of Ngamsurach et al., which supported the addition of iron(III) oxide-hydroxide into bagasse, and bagasse fly ash had higher RB4 dye removal efficiency than the addition of zinc oxide into the same raw materials.⁷ Moreover, the study of Praipipat et al. found that the chicken and duck eggshell beads modified with iron(III) oxide-hydroxide also presented higher RB4 dye removal than the addition of zinc oxide into the same raw materials.²⁴ In addition, other studies also reported that the addition of iron oxide or magnetite (Fe_3O_4) in carboxymethyl cellulose helped in the increase of the dye removal efficiency.^{25,26} Furthermore, the study of Noreen et al. also supported that the addition of Fe_2O_3 into the extracted *Cassia Fistula* gave a higher direct golden yellow removal than ZnO and CuO.²⁷ Therefore, LBF was a potential adsorbent material for dye removal and could be used as an alternative adsorbent for wastewater treatment in the future.

2.4. Isotherm Study. The plotting of linear and nonlinear models of Langmuir, Freundlich, Temkin, and Dubinin–Radushkevich isotherms was used to determine the adsorption pattern of LBF and LBZ. For linear models, Langmuir, Freundlich, Temkin, and Dubinin–Radushkevich isotherms were plotted by C_e/q_e versus C_e , $\log q_e$ versus $\log C_e$, q_e versus $\ln C_e$, and $\ln q_e$ versus ε^2 , respectively. For nonlinear models, all isotherms were plotted by C_e versus q_e . The plotting results and the equilibrium isotherm parameters are demonstrated in Figure 7a–e and Table 2, respectively.

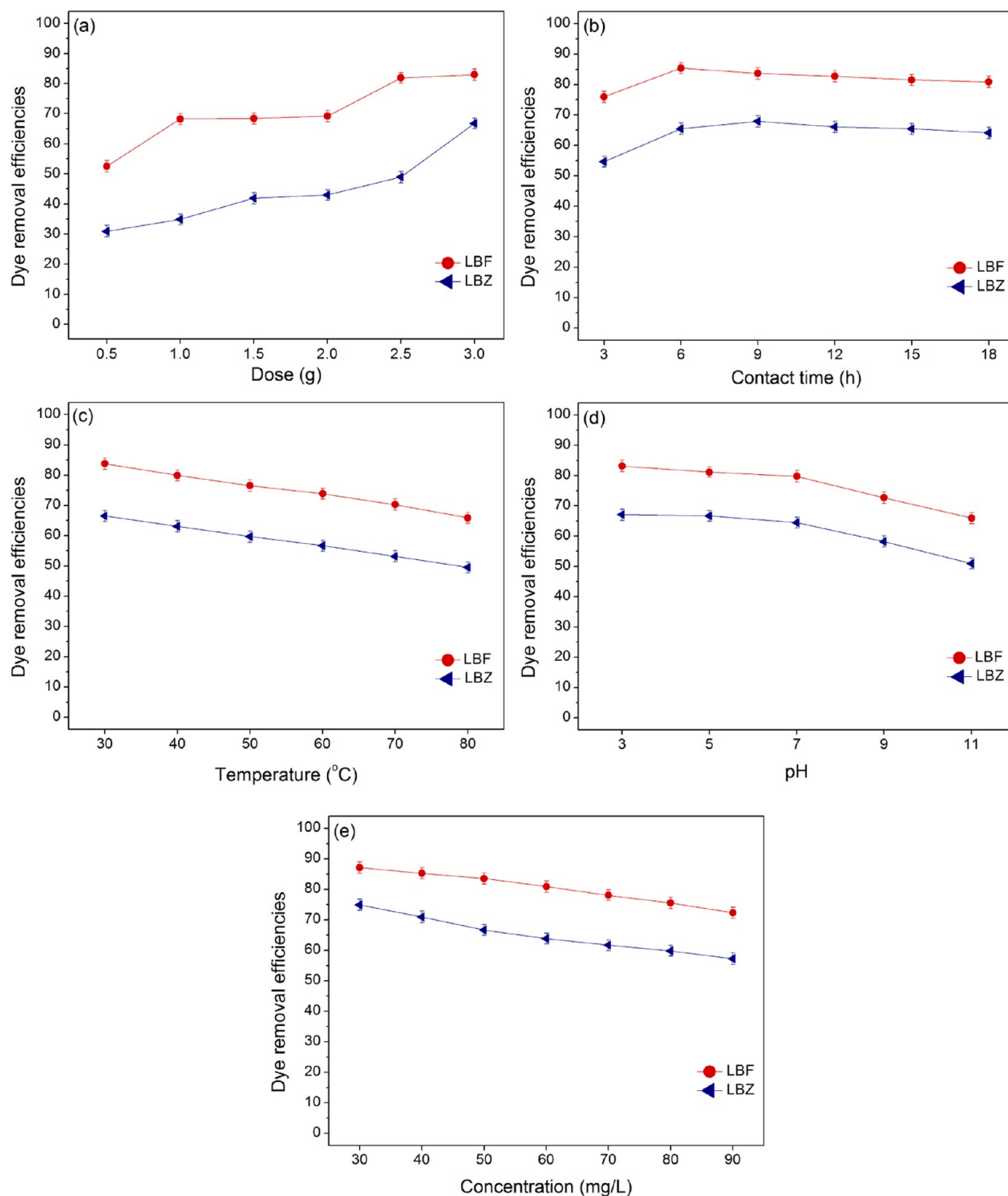


Figure 6. Batch experiments of LBF and LBZ in the (a) dose, (b) contact time, (c) temperature, (d) pH, and (e) concentration for RB4 dye adsorptions with the control condition of the initial RB4 dye concentration of 50 mg/L, a sample volume of 100 mL, and a shaking speed of 150 rpm.

For the linear Langmuir model, the Langmuir maximum adsorption capacities (q_m) of LBF and LBZ were 3.229 and 2.589 mg/g, and Langmuir adsorption constants (K_L) of LBF and LBZ were 0.091 and 0.050 L/mg, respectively. For the nonlinear Langmuir model, the Langmuir maximum adsorption capacities (q_m) of LBF and LBZ were 3.239 and 2.617 mg/g, and Langmuir adsorption constants (K_L) of LBF and LBZ were 0.090 and 0.049 L/mg, respectively. For the linear

Freundlich isotherm, the $1/n$ values of LBF and LBZ were 0.449 and 0.268. Freundlich adsorption constants (K_F) of LBF and LBZ were 0.518 and 0.514 (mg/g)(L/mg) $^{1/n}$. For the nonlinear Freundlich isotherm, the $1/n$ values of LBF and LBZ were 0.464 and 0.270. Freundlich adsorption constants (K_F) of LBF and LBZ were 0.505 and 0.512 (mg/g)(L/mg) $^{1/n}$. For the linear Temkin isotherm, b_T values of LBF and LBZ were 3337.822 and 4167.999 J/mol. A_T values of LBF and LBZ were

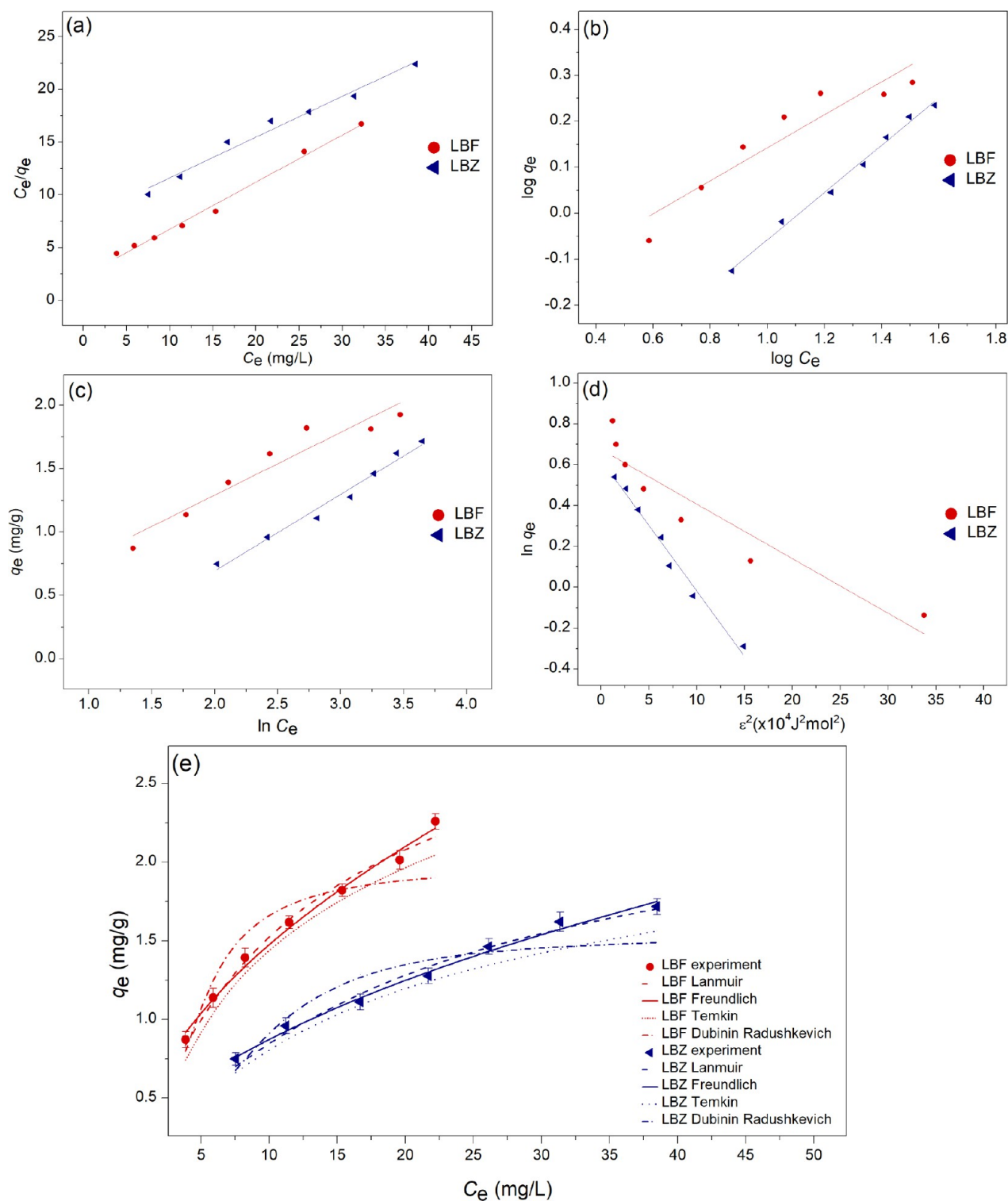


Figure 7. (a) Linear Langmuir, (b) linear Freundlich, (c) linear Temkin, (d) linear Dubinin–Radushkevich, and (e) nonlinear adsorption isotherms of LBF and LBZ for RB4 dye adsorptions.

0.778 and 0.426 L/g. For the nonlinear Temkin isotherm, the b_T values of LBF and LBZ were 3381.262 and 4564.646 J/mol. A_T values of LBF and LBZ are 0.701 and 0.440 L/g. For the linear Dubinin–Radushkevich model, the maximum adsorption capacities (q_m) of LBF and LBZ were 1.964 and 1.542 mg/g, and the activity coefficient (K_{DR}) values of both materials were 0.027 and 0.081 mol²/J². The adsorption energy (E) values of LBF and LBZ were 4.327 and 2.486 kJ/mol. For

the nonlinear Dubinin–Radushkevich model, the maximum adsorption capacities (q_m) of LBF and LBZ were 1.712 and 1.319 mg/g, and the activity coefficient (K_{DR}) values of both materials were 0.022 and 0.061 mol²/J². The adsorption energy (E) values of LBF and LBZ were 4.784 and 2.866 kJ/mol.

For R^2 value consideration, the R^2 values of LBF and LBZ in the linear Langmuir model were 0.986 and 0.980 and in the linear Freundlich model were 0.992 and 0.993. For the linear

Table 2. Equilibrium Isotherm Parameters of LBF and LBZ for RB4 Dye Adsorptions

regression method	isotherm model	parameter	LBF	LBZ		
linear	Langmuir	q_m (mg/g)	3.229	2.589		
		K_L (L/mg)	0.091	0.050		
		R^2	0.986	0.980		
	Freundlich	$1/n$	0.449	0.268		
		K_F (mg/g) (L/mg) ^{1/n}	0.518	0.514		
		R^2	0.992	0.993		
	Temkin	b_T (J/mol)	3337.822	4167.999		
		A_T (L/g)	0.778	0.426		
		R^2	0.987	0.979		
	Dubinin–Radushkevich	q_m (mg/g)	1.964	1.542		
		K_{DR} (mol ² /J ²)	0.027	0.081		
		E (kJ/mol)	4.327	2.486		
		R^2	0.882	0.856		
		nonlinear	Langmuir	q_m (mg/g)	3.239	2.617
				K_L (L/mg)	0.090	0.049
R^2	0.987			0.982		
R_{adj}^2	0.984			0.978		
RMSE	0.061			0.052		
Freundlich	$1/n$			0.464	0.270	
	K_F (mg/g) (L/mg) ^{1/n}		0.505	0.512		
	R^2		0.992	0.992		
	R_{adj}^2		0.990	0.990		
	RMSE		0.049	0.036		
	Temkin		b_T (J/mol)	3381.262	4564.646	
A_T (L/g)			0.701	0.440		
R^2			0.989	0.977		
R_{adj}^2			0.987	0.973		
RMSE			0.068	0.060		
Dubinin–Radushkevich		q_m (mg/g)	1.712	1.319		
		K_{DR} (mol ² /J ²)	0.022	0.061		
		E (kJ/mol)	4.784	2.866		
		R^2	0.897	0.857		
	R_{adj}^2	0.877	0.828			
	RMSE	0.212	0.164			

Temkin model, R^2 values of LBF and LBZ were 0.987 and 0.979, and for the linear Dubinin–Radushkevich model, they were 0.882 and 0.856. In addition, R^2 values of LBF and LBZ in the nonlinear Langmuir model were 0.987 and 0.982, and in the nonlinear Freundlich model were 0.992 and 0.992. For the nonlinear Temkin model, R^2 values of LBF and LBZ were 0.989 and 0.977, and those of the nonlinear Dubinin–Radushkevich model were 0.897 and 0.857. Moreover, the R_{adj}^2 of LBF and LBZ in the nonlinear Langmuir model were 0.984 and 0.978, and the R_{adj}^2 of LBF and LBZ in the nonlinear Freundlich model were 0.990 and 0.990. R_{adj}^2 of LBF and LBZ in the nonlinear Temkin model were 0.987 and 0.973, and those in the nonlinear Dubinin–Radushkevich model were 0.877 and 0.828. Since R^2 values of LBF and LBZ in both linear and nonlinear Freundlich models were higher than those in Langmuir, Temkin, and Dubinin–Radushkevich models, their adsorption patterns corresponded to the Freundlich isotherm, relating to physiochemical adsorption. Freundlich's parameters of a constant depiction of the adsorption intensity ($1/n$) and Freundlich adsorption constant (K_F) are used for explaining the RB4 dye adsorption pattern of LBF and LBZ. For a $1/n$ value, a higher $1/n$ value means higher RB4 dye adsorption, in which case LBF demonstrated a higher $1/n$ value than LBZ. In addition, since both materials had $1/n$ values in a range of 0–1, it means that they were favorable

adsorption isotherms. For a K_F value, LBF also illustrated a higher K_F value than LBZ, so LBF might have had higher RB4 dye adsorption than LBZ, which corresponded to a $1/n$ value. Moreover, both linear and nonlinear isotherm models were recommended to plot graphs for confirming the results and protecting against data mistranslation.^{28–30}

2.5. Kinetic Study. The plotting of linear and nonlinear kinetic models of pseudo-first-order, pseudo-second-order, Elovich models, and intra-particle diffusion was used to investigate the adsorption rate and mechanism of LBF and LBZ. For linear models, the pseudo-first-order kinetic model, pseudo-second-order kinetic model, Elovich model, and intra-particle diffusion model were plotted by $\ln(q_e - q_t)$ versus time (t), t/q_t versus time (t), q_t versus $\ln t$, and q_t versus time ($t^{0.5}$), respectively. For nonlinear models, they were plotted by q_t versus time (t). The plotting results and the adsorption kinetic parameters are demonstrated in Figure 8a–e and Table 3, respectively.

For the linear pseudo-first-order kinetic model, the adsorption capacities (q_e) of LBF and LBZ were 0.248 and 0.467 mg/g, and the reaction of rate constants (k_1) of LBF and LBZ were 0.001 and 0.004 min⁻¹. For the nonlinear pseudo-first-order kinetic model, the adsorption capacities (q_e) of LBF and LBZ were 0.268 and 0.504 mg/g, and the reaction of rate constants (k_1) of LBF and LBZ were 0.002 and 0.006 min⁻¹.

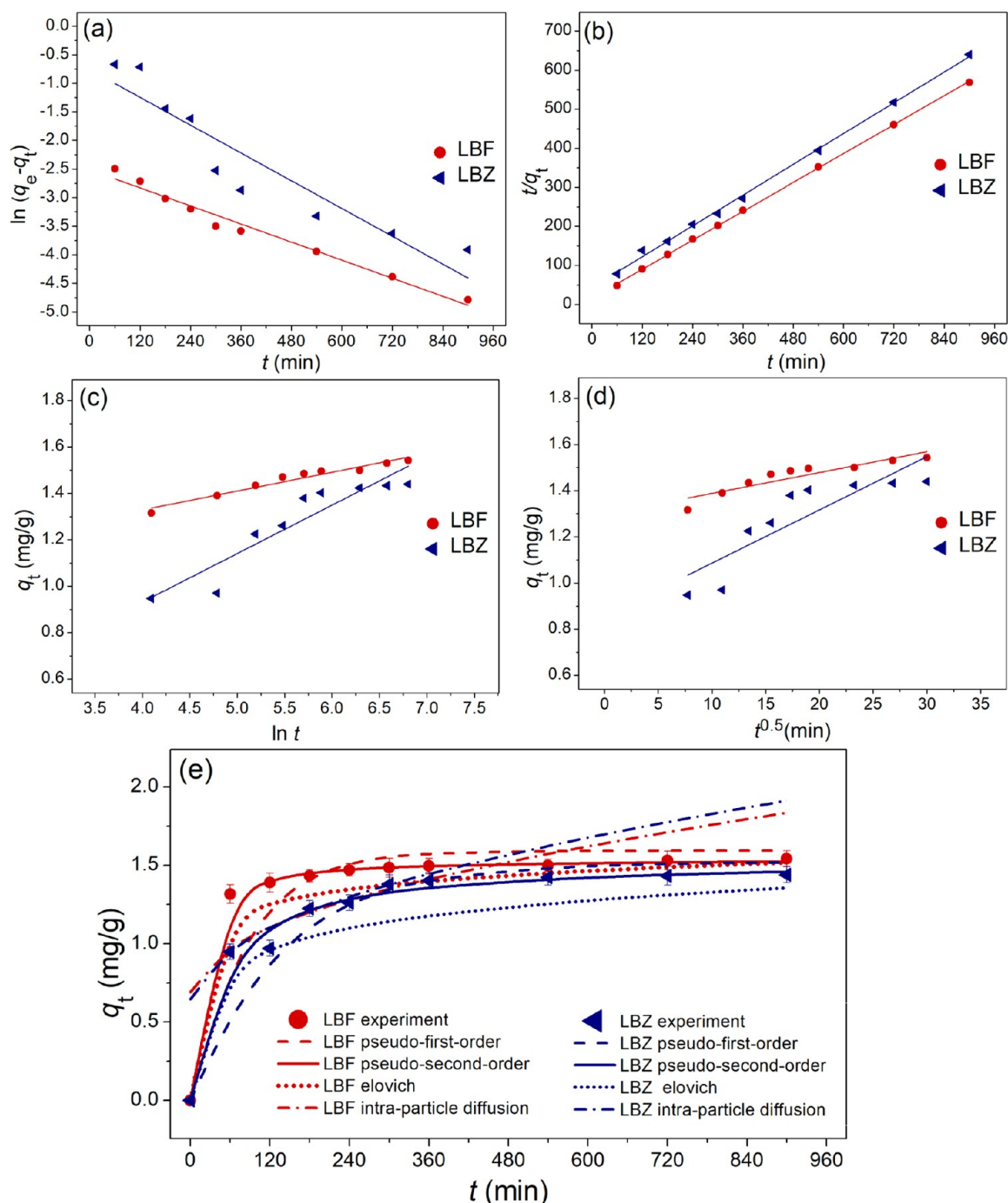


Figure 8. (a) Linear pseudo-first-order, (b) linear pseudo-second-order, (c) linear Elovich model, (d) linear intra-particle diffusion, and (e) nonlinear kinetic models of LBF and LBZ for RB4 dye adsorptions.

For the linear pseudo-second-order kinetic model, the adsorption capacities (q_e) of LBF and LBZ were 1.562 and 1.523 mg/g, and the reaction of rate constants (k_2) of LBF and LBZ was 0.042 and 0.015 g/mg·min. For the nonlinear pseudo-second-order kinetic model, the adsorption capacities (q_e) of LBF and LBZ were 1.562 and 1.534 mg/g, respectively, and the reaction of rate constants (k_2) of LBF and LBZ was 0.042 and 0.014 g/mg/min, respectively. For the linear Elovich model, the initial adsorption rates (α) of LBF and LBZ were 140.303 and 1.345 mg/g/min, and the extents of surface coverage (β) of LBF and LBZ were 12.361 and 4.789 g/mg. For the nonlinear Elovich model, the initial adsorption rates

(α) of LBF and LBZ were 142.599 and 1.232 mg/g/min, and the extents of surface coverage (β) of LBF and LBZ were 11.310 and 4.382 g/mg, respectively. For the linear intra-particle diffusion model, the reaction of rate constants (k_i) of LBF and LBZ were 0.009 and 0.024 mg/g·min^{0.5}, and the constant C_i values of LBF and LBZ were 1.283 and 0.856 mg/g. For the nonlinear intra-particle diffusion model, the reaction of rate constants (k_i) of LBF and LBZ were 0.008 and 0.022 mg/g·min^{0.5}, and the constant C_i values of LBF and LBZ were 1.174 and 0.783 mg/g.

For R^2 value consideration, R^2 values of LBF and LBZ in the linear pseudo-first-order kinetic model were 0.868 and 0.874

Table 3. Adsorption Kinetic Parameters of LBF and LBZ for RB4 Dye Adsorptions

regression method	model	parameter	LBF	LBZ	
linear	pseudo-first-order kinetic model	q_e (mg/g)	0.248	0.467	
		k_1 (min ⁻¹)	0.001	0.004	
		R^2	0.868	0.874	
	pseudo-second-order kinetic model	q_e (mg/g)	1.562	1.523	
		k_2 (g/mg·min)	0.042	0.015	
		R^2	1.000	0.998	
	Elovich model	α (mg/g/min)	140.303	1.345	
		β (g/mg)	12.361	4.789	
		R^2	0.954	0.868	
	intra-particle diffusion	k_i (mg/g·min ^{0.5})	0.009	0.024	
		C_i (mg/g)	1.283	0.856	
		R^2	0.844	0.756	
	nonlinear	pseudo-first-order kinetic model	q_e (mg/g)	0.268	0.504
			k_1 (min ⁻¹)	0.002	0.006
			R^2	0.859	0.885
R_{adj}^2			0.841	0.870	
RMSE			0.186	0.160	
pseudo-second-order kinetic model		q_e (mg/g)	1.562	1.534	
		k_2 (g/mg·min)	0.042	0.014	
		R^2	0.999	0.998	
		R_{adj}^2	0.999	0.997	
		RMSE	0.015	0.062	
Elovich model		α (mg/g/min)	142.599	1.232	
		β (g/mg)	11.310	4.382	
		R^2	0.952	0.872	
		R_{adj}^2	0.946	0.856	
		RMSE	0.109	0.168	
intra-particle diffusion		k_i (mg/g·min ^{0.5})	0.008	0.022	
		C_i (mg/g)	1.174	0.783	
		R^2	0.846	0.759	
		R_{adj}^2	0.826	0.729	
		RMSE	0.336	0.321	

and in the linear pseudo-second-order kinetic model were 1.000 and 0.998. In addition, R^2 values of LBF and LBZ of the linear Elovich model were 0.954 and 0.868 and in the linear intra-particle model were 0.844 and 0.756. In addition, R^2 values of LBF and LBZ in the nonlinear pseudo-first-order kinetic model were 0.859 and 0.885, and in the nonlinear pseudo-second-order kinetic model were 0.999 and 0.998. Moreover, R^2 values of LBF and LBZ of the nonlinear Elovich model were 0.952 and 0.872 and in the nonlinear intra-particle model were 0.846 and 0.759. Moreover, the R_{adj}^2 of LBF and LBZ in the nonlinear pseudo-first-order kinetic model were 0.841 and 0.870, and the R_{adj}^2 of LBF and LBZ in the nonlinear pseudo-second-order kinetic model were 0.999 and 0.997. In addition, R_{adj}^2 of LBF and LBZ in the nonlinear Elovich model were 0.946 and 0.856, and R_{adj}^2 of the nonlinear intra-particle diffusion model were 0.826 and 0.729. Since R^2 values of LBF and LBZ in both linear and nonlinear pseudo-second-order kinetic models were higher than in the pseudo-first-order kinetic, Elovich, and intra-particle diffusion models, the adsorption rate and mechanism of all dye-adsorbent materials corresponded to the pseudo-second-order kinetic models, relating to the chemisorption process with heterogeneous adoption. A pseudo-second-order kinetic model's parameters of adsorption capacity (q_e) and the pseudo-second-order kinetic rate constant (k_2) are used to illustrate the adsorption rate and mechanism of LBF and LBZ. Since both the q_e and k_2 values of LBF were higher than those of LBZ, LBF might

adsorb RB4 dye at a reaction rate faster than that of LBZ. Finally, the plotting of both linear and nonlinear kinetic models was also recommended for correct data translations.^{28–30}

2.6. Desorption Experiment. The reusability of materials is an important test to investigate the cost and economic feasibility of industrial applications using the desorption experiment. LBF and LBZ were used for the desorption experiments with five adsorption–desorption cycles to confirm their abilities for RB4 dye removal, and their results are illustrated in Figure 9a,b. In Figure 9a, LBF could be reused in five cycles with high adsorption and desorption in the ranges of 60.52–83.05 and 52.42–83.20%, respectively, where adsorption and desorption were decreased by approximately 23 and 30%. For LBZ, it was also confirmed to be reusable in five cycles with high adsorption and desorption in the ranges of 66.64–40.80 and 34.11–66.20%, respectively, where adsorption and desorption were decreased by approximately 26 and 32%, respectively, shown in Figure 9b. Therefore, LBF and LBZ are potential materials for RB4 dye removal with a reusability of more than five cycles, and they can be applied to industrial applications in the future.

2.7. Analysis of Cost-Effectiveness. The analysis of cost-effectiveness is a beneficial idea that considers the cost and economic value of materials before applying them in future industrial applications. The main factors of availability of raw material, synthesis methods, reusability, and ease of operation are used for choosing the adsorbent. First, since the raw

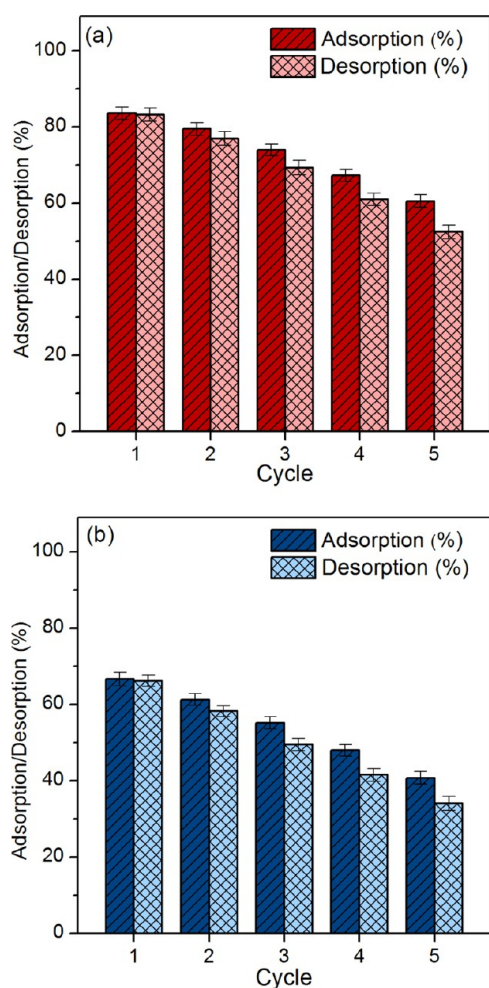


Figure 9. Desorption experiments of (a) LBF and (b) LBZ.

material of LBF and LBZ is lemon peels, they are food wastes and have easy availability, so in regard to them, there is no cost for raw materials. Moreover, this also helps to reduce waste management problems by using recycled food waste for another purpose. Second, the synthesis method of LBF and LBZ is not complicated considering the suitable cost of chemicals, since the cost of materials was approximately 20 USD per kg. Third, LBF and LBZ could be reused for more than five cycles, with RB4 dye adsorptions of more than 41%. Finally, since LBF and LBZ are beaded materials, they are easily separated after water treatment. This helps to save an operation from costing more than the powder adsorbent. Therefore, LBF and LBZ are good options as RB4 dye adsorbents for industrial applications.

3. CONCLUSIONS

This study synthesized two dye-adsorbent materials of LBF and LBZ for RB4 dye adsorption in an aqueous solution. Both materials had a spherical shape with a coarse surface. LBF had an iron-rust beaded color, whereas LBZ had a light-yellow beaded color. Both materials demonstrated semicrystalline structures with specific peaks of sodium alginate and specific peaks of iron(III) oxide-hydroxide and zinc oxide in LBF and LBZ, respectively. Their surface morphologies had a spherical shape with coarse surfaces, and chemical elements of carbon (C), oxygen (O), calcium (Ca), chlorine (Cl), and sodium (Na) were found in both materials. Iron (Fe) was also detected

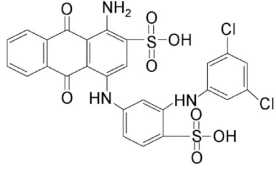
in LBF, and zinc (Zn) was found in LBZ. Six main functional groups of O–H, C≡N, C=C, C–OH, C–O–C, and C–H were detected in both materials. For batch experiments, LBF demonstrated higher RB4 dye removal efficiency than LBZ, and their optimum conditions for the highest RB4 dye adsorptions at a concentration of 50 mg/L were 3 g, 6 h, 30 °C, and pH 3 for LBF and 3 g, 9 h, 30 °C, and pH 3 for LBZ. As a result, the addition of iron(III) oxide-hydroxide into lemon peel beads helped in increasing the material efficiency more than zinc oxide because of less spent adsorption time. For adsorption isotherms and kinetics, they corresponded to the Freundlich model and pseudo-second-order kinetic models relating to physiochemical adsorption and the chemisorption process. Therefore, LBF was the potential material for RB4 dye adsorption, and it might be used for industrial applications. For future work, competing ions such as magnesium (Mg^{2+}), sodium (Na^+), and natural organic matter (NOM) contaminated in real wastewater or natural water should be investigated, and the continuous flow study also requires studying of feasible applications in industrial wastewater treatment.

4. MATERIALS AND METHODS

4.1. Raw Materials and Preparations. Lemon peels were collected from the local markets in Khon Kaen province, Thailand. They were washed with distilled water (DW) many times to remove contaminants before use.³¹

4.2. Chemicals. All chemicals were of analytical grade (AR) without purification before use. For modified bead materials, ferric chloride hexahydrate ($FeCl_3 \cdot 6H_2O$) (LOBA, India), sodium hydroxide (NaOH) (RCI Labscan, Thailand), and zinc oxide (ZnO) (QRëC, New Zealand) were used. Sodium alginate ($NaC_6H_7O_6$) (Merck, Germany) and calcium chloride ($CaCl_2$) (Kemaus, New Zealand) were used for bead formation. For the preparation of synthetic dye solution, RB4 dye ($C_{23}H_{14}Cl_2N_6O_8S_2$) (Sigma-Aldrich, Germany) was used, and its structure is illustrated in Table 4. Finally, 0.5% of 65% nitric acid (HNO_3) (Merck, Germany) and 0.5% of NaOH (RCI Labscan, Thailand) were used for pH adjustment.

Table 4. Characteristics and Chemical Structure of RB4

Characteristics and chemical structure	
Chemical class	Anionic
Chemical name	Reactive blue 4 (RB4)
Chemical formula	$C_{23}H_{14}Cl_2N_6O_8S_2$
Molecular weight (g/mol)	637.43
(λ_{max}) (nm)	595
Chemical structure	

4.3. Preparation of Dye Solution. The dye solutions from 30 to 90 mg/L were prepared from the stock solution of RB4 dye at a 100 mg/L concentration.

4.4. Material Synthesis. The syntheses of LBF and LBZ are described in Figure 10, and the details are clearly explained below.

4.4.1. Synthesis of LBF. The synthesis method of this material is based on Threpanich and Praipipat.³¹ First, 40 g of lemon peels were soaked in the mixed solution of ethanol

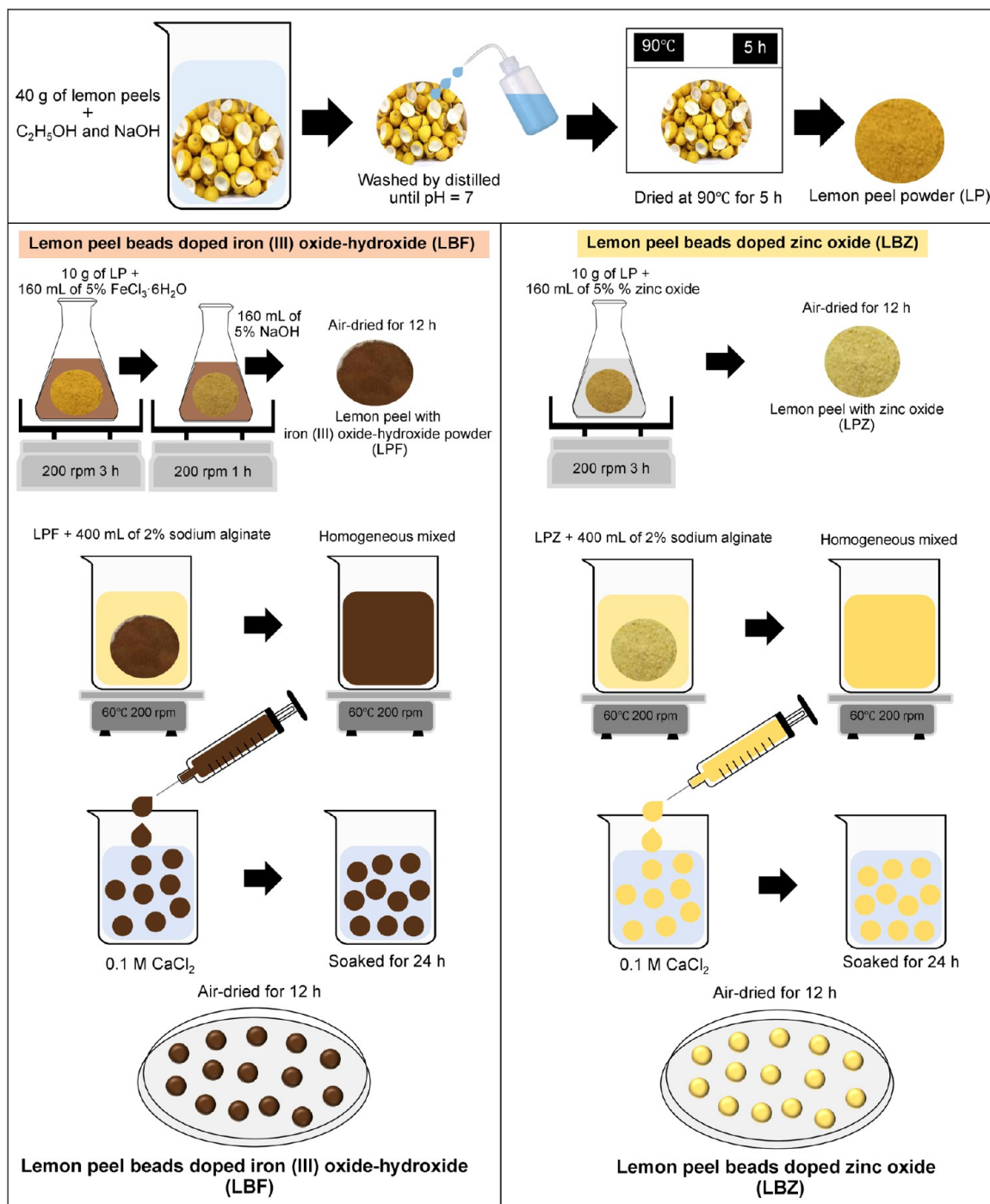


Figure 10. Synthesis of LBF and LBZ.

(C₂H₅OH) and 0.5 M sodium hydroxide (NaOH) in a ratio of 2:1 for 12 h. Then, they were washed with DW until the pH of the water solution was equal to 7. The samples were dried at 90 °C for 5 h in a hot air oven (Binder, FED 53, Germany). After that, the samples were crushed into small pieces, sieved to a size of 125 μm, kept in a desiccator before use, and called LP. Second, 10 g of LP was added to a 500 mL Erlenmeyer flask containing 160 mL of FeCl₃·6H₂O, and they were mixed using an orbital shaker (GFL, 3020, Germany) of 200 rpm for 3 h. Then, they were filtered and air-dried at 12 h. Next, they were added to a 500 mL Erlenmeyer flask containing 160 mL of 5% NaOH, and they were mixed using an orbital shaker at

200 rpm for 1 h. After that, they were filtrated, air-dried for 12 h, kept in desiccators before use, and called LPF. Third, LPF were added to 400 mL of 2% sodium alginate, and then they were homogeneously mixed and heated on a hot plate (Ingenieurbüro CAT, M. Zipperer GmbH, M 6, Germany) at 60 °C with constant stirring at 200 rpm. Then, the samples were added dropwise into 250 mL of 0.1 M CaCl₂ by using a 10 mL syringe with a needle size of 1.2 × 40 mm. The beaded samples were soaked in 0.1 M CaCl₂ for 24 h, and then they were filtered and rinsed with DI water. After that, they were air-dried at room temperature for 12 h and kept in desiccators before use called LBF.

4.4.2. Synthesis of LBZ. First, 10 g of LP was added to a 500 mL Erlenmeyer flask containing 160 mL of 5% zinc oxide, and the samples were mixed using an orbital shaker at 200 rpm for 3 h. Then, they were filtered, air-dried at 12 h, kept in a desiccator, and called LPZ. Second, LPZ was added to 400 mL of 2% sodium alginate, and then they were homogeneously mixed and heated on a hot plate at 60 °C with constant stirring at 200 rpm. Third, the samples were added dropwise into 250 mL of 0.1 M CaCl₂ by using a 10 mL syringe with a needle size of 1.2 × 40 mm. The beaded samples were soaked in 0.1 M CaCl₂ for 24 h, and then they were filtered and rinsed with DI water. Finally, they were air-dried at room temperature for 12 h, kept in desiccators before use, and called LBZ.

4.5. Characterizations of LBF and LBZ. Characterizations of LBF and LBZ were investigated by XRD (Bruker, D8 Advance, Switzerland), FESEM–FIB with EDX (FEI, Helios NanoLab G3 CX, USA), FTIR spectroscopy (Bruker, Tensor 27, Hong Kong), and Zetasizer Nano (Malvern, Zetasizer Nano ZS, UK) for identifying crystalline structures, surface morphologies, chemical compositions, functional groups, and ζ potentials, respectively.

4.6. Batch Experiments. Since affecting parameters of the dose, contact time, temperature, pH, and dye concentration might affect RB4 dye removal efficiencies on LBF and LBZ, batch experiments were designed to investigate how much they affect finding the optimum condition that obtains the highest dye removal efficiency of each material. The varying dosages of 0.5–3 g, contact times of 3–18 h, temperatures of 30–80 °C, pH values of 3, 5, 7, 9, and 11, and the dye concentration of 30–90 mg/L, with the control conditions of a shaking speed of 150 rpm and a sample volume of 100 mL, were used, and dye concentrations were analyzed using a UV–vis spectrophotometer (Hitachi, UH5300, Japan). Triplicate experiments were conducted to confirm the results, and the average values were reported. Dye removal efficiency in the percentage was calculated by eq 1.

$$\text{Dye removal efficiency (\%)} = ((C_0 - C_e)/C_0) \times 100 \quad (1)$$

where C_e is the equilibrium of the dye concentration (mg/L), and C_0 is the initial dye concentration (mg/L).

4.7. Adsorption Isotherms. To understand the adsorption patterns of LBF and LBZ, adsorption isotherms of linear and nonlinear Langmuir, Freundlich, Temkin, and Dubinin–Radushkevich isotherms were conducted following eqs 2–9^{32–35}

Langmuir isotherm

$$\text{linear: } C_e/q_e = 1/q_m K_L + C_e/q_m \quad (2)$$

$$\text{nonlinear: } q_e = q_m K_L C_e / (1 + K_L C_e) \quad (3)$$

Freundlich isotherm

$$\text{linear: } \log q_e = \log K_F + 1/n \log C_e \quad (4)$$

$$\text{Nonlinear: } q_e = K_F C_e^{1/n} \quad (5)$$

Temkin isotherm

$$\text{linear: } q_e = RT/b_T \ln A_T + RT/b_T \ln C_e \quad (6)$$

$$\text{nonlinear: } q_e = RT/b_T \ln A_T C_e \quad (7)$$

Dubinin–Radushkevich isotherm

$$\text{linear: } \ln q_e = \ln q_m - K_{DR} \varepsilon^2 \quad (8)$$

$$\text{nonlinear: } q_e = q_m \exp(-K_{DR} \varepsilon^2) \quad (9)$$

where q_e is the capacity of dye adsorption on LBF or LBZ at equilibrium (mg/g), q_m is the maximum amount of dye adsorption on LBF or LBZ (mg/g), C_e is the equilibrium of dye concentration (mg/L), K_L is the Langmuir adsorption constant (L/mg), K_F is the Freundlich constant of adsorption capacity (mg/g) (L/mg)^{1/n}, and n is the constant depicting adsorption intensity.³⁶ R is the universal gas constant (8.314 J/mol K), T is the absolute temperature (K), b_T is the constant related to the heat of adsorption (J/mol), and A_T is the equilibrium binding constant corresponding to maximum binding energy (L/g). K_{DR} is the activity coefficient related to mean adsorption energy (mol²/J²), and ε is the Polanyi potential (J/mol).³¹ Graphs of linear Langmuir, Freundlich, Temkin, and Dubinin–Radushkevich isotherms were plotted by C_e/q_e versus C_e , $\log q_e$ versus $\log C_e$, q_e versus $\ln C_e$, and $\ln q_e$ versus ε^2 , respectively, whereas graphs of their nonlinear models were plotted by q_e versus C_e .

For the adsorption isotherm experiment, the optimum dose of LBF or LBZ was applied with various RB4 dye concentrations ranging from 30 to 90 mg/L with the control condition of a water sample of 100 mL, a contact time of 12 h, a temperature of 30 °C, a pH of 3, and a shaking speed of 150 rpm.

4.8. Adsorption Kinetics. Adsorption kinetics in both linear and nonlinear pseudo-first-order, pseudo-second-order, Elovich, and intra-particle diffusion models following eqs 10–16^{37–40} were studied to understand the adsorption rate and mechanism of LBF and LBZ.

Pseudo-first-order kinetic model

$$\text{linear: } \ln(q_e - q_t) = \ln q_e - k_1 t \quad (10)$$

$$\text{nonlinear: } q_t = q_e (1 - e^{-k_1 t}) \quad (11)$$

Pseudo-second-order kinetic model

$$\text{linear: } t/q_t = 1/k_2 q_e^2 + (t/q_e) \quad (12)$$

$$\text{nonlinear: } q_t = k_2 q_e^2 t / (1 + q_e k_2 t) \quad (13)$$

Elovich model

$$\text{linear: } q_t = (1/\beta) \ln \alpha \beta + (1/\beta) \ln t \quad (14)$$

$$\text{nonlinear: } q_t = \beta \ln t + \beta \ln \alpha \quad (15)$$

Intra-particle diffusion model

$$\text{linear and nonlinear: } q_t = k_i t^{0.5} + C_i \quad (16)$$

where q_e (mg/g) and q_t (mg/g) are the capacities of dyes adsorbed by LBF or LBZ at equilibrium and at time (t), respectively. k_1 (min⁻¹), k_2 (g/mg•min), α (mg/g/min), and k_i (mg/g•min^{0.5}) are the reaction of rate constants of pseudo-first-order, pseudo-second-order, Elovich, and intra-particle diffusion models, respectively. β is the extent of surface coverage (g/mg), and C_i is the constant that gives an idea about the thickness of the boundary layer (mg/g).³¹ Graphs of linear pseudo-first-order, pseudo-second-order, Elovich, and intra-particle diffusion models were plotted by $\ln(q_e - q_t)$ versus time (t), t/q_t versus time (t), q_t versus $\ln t$, and q_t versus time ($t^{0.5}$), respectively, whereas their nonlinear graphs were

plotted by the capacity of dye adsorbed by LBF or LBZ at the time (q_t) versus time (t).

For the adsorption kinetic experiment, the optimum dose of LBF or LBZ was applied with the control conditions of an RB4 dye concentration of 50 mg/L, a sample volume of 1000 mL, a contact time of 15 h, a temperature of 30 °C, a pH of 3, and a shaking speed of 150 rpm.

4.9. Desorption Experiment. The desorption experiment is designed to investigate the possible material reusability by studying five adsorption–desorption cycles to confirm the abilities of LBF and LBZ for RB4 dye removal. After the adsorption process, LFB or LBZ was added to 250 mL of the Erlenmeyer flask containing 100 mL of 0.01 M NaOH solution, and then it was shaken with an incubator shaker (New Brunswick, Innova 42, USA) at 150 rpm for 2 h with a temperature of 30 °C. After that, it was washed with deionization water and dried at room temperature, and LFB or LBZ is ready for the next adsorption cycle. The desorption efficiency in percentage is calculated following eq 17.

$$\text{Desorption (\%)} = (q_d/q_a) \times 100 \quad (17)$$

where q_d is the amount of RB4 dye desorbed (mg/mL) and q_a is the amount of RB4 dye adsorbed (mg/mL).

AUTHOR INFORMATION

Corresponding Author

Pornsawai Praipipat – Department of Environmental Science, Khon Kaen University, Khon Kaen 40002, Thailand; Environmental Applications of Recycled and Natural Materials (EARN) Laboratory, Khon Kaen University, Khon Kaen 40002, Thailand; orcid.org/0000-0003-1311-2071; Email: pornprai@kku.ac.th

Authors

Pimployp Ngamsurach – Department of Environmental Science, Khon Kaen University, Khon Kaen 40002, Thailand; Environmental Applications of Recycled and Natural Materials (EARN) Laboratory, Khon Kaen University, Khon Kaen 40002, Thailand

Vatcharaporn Prasongdee – Department of Environmental Science, Khon Kaen University, Khon Kaen 40002, Thailand

Complete contact information is available at:

<https://pubs.acs.org/10.1021/acsomega.2c05956>

Author Contributions

P.P.: supervision, conceptualization, funding acquisition, investigation, methodology, validation, visualization, writing—original draft, writing—reviewing, and editing. P.N.: visualization, writing—original draft. V.P.: investigation.

Notes

The authors declare no competing financial interest.

The raw/processed data required to reproduce these findings cannot be shared at this time due to legal or ethical reasons. The raw/processed data required to reproduce these findings cannot be shared at this time as the data also forms part of an ongoing study.

ACKNOWLEDGMENTS

The authors are grateful for the financial support received from The Office of the Higher Education Commission and The Thailand Research Fund grant (MRG6080114), Coordinating Center for Thai Government Science and Technology

Scholarship Students (CSTS), the National Science and Technology Development Agency (NSTDA) Fund grant (SCHNR2016-122), and Research and Technology Transfer Affairs of Khon Kaen University.

REFERENCES

- (1) Al-Tohamy, R.; Ali, S. S.; Li, F.; Okasha, K. M.; Mahmoud, Y. A. G.; Elsamahy, T.; Jiao, H.; Fu, Y.; Sun, J. A Critical Review on the Treatment of Dye-Containing Wastewater: Ecotoxicological and Health Concerns of Textile Dyes and Possible Remediation Approaches for Environmental Safety. *Ecotoxicol. Environ. Saf.* **2022**, *231*, 113160.
- (2) Lellis, B.; Fávoro-Polonio, C. Z.; Pamphile, J. A.; Polonio, J. C. Effects of Textile Dyes on Health and the Environment and Bioremediation Potential of Living Organisms. *Biotechnol. Res. Int.* **2019**, *3*, 275–290.
- (3) Chavan, R. B.16—Environmentally Friendly Dyes. In *Woodhead Publishing Series in Textiles*; Clark, M., Ed.; Woodhead Publishing, 2011; Vol. 1, pp 515–561.
- (4) Samsami, S.; Mohamadizani, M.; Sarrafzadeh, E. R.; Rene, M.; Firoozbahr, M. Recent Advances in the Treatment of Dye-Containing Wastewater from Textile Industries: Overview and Perspectives. *Process Saf. Environ. Prot.* **2020**, *143*, 138–163.
- (5) Bukhari, A.; Ijaz, I.; Zain, H.; Gilani, E.; Nazir, A.; Bukhari, A.; Raza, S.; Ansari, J.; Hussain, S.; Alarfaji, S. S.; Saeed, R.; Naseer, Y.; Aftab, R.; Iram, S. Removal of Eosin Dye from Simulated Media onto Lemon Peel-Based Low Cost Biosorbent. *Arabian J. Chem.* **2022**, *15*, 103873.
- (6) Zeng, S.; Long, J.; Sun, J.; Wang, G.; Zhou, L. A Review on Peach Gum Polysaccharide: Hydrolysis, Structure, Properties and Applications. *Carbohydr. Polym.* **2022**, *279*, 119015.
- (7) Ngamsurach, P.; Nemkhuntod, S.; Chanaphan, P.; Praipipat, P. Modified Beaded Materials from Recycled Wastes of Bagasse and Bagasse Fly Ash with Iron (III) Oxide-Hydroxide and Zinc Oxide for the Removal of Reactive Blue 4 Dye in Aqueous Solution. *ACS Omega* **2022**, *7*, 34839–34857.
- (8) Sharifzade, G.; Asghari, A.; Rajabi, M. Highly Effective Adsorption of Xanthene Dyes (Rhodamine B and Erythrosine B) from Aqueous Solutions onto Lemon Citrus Peel Active Carbon: Characterization, Resolving Analysis, Optimization and Mechanistic Studies. *RSC Adv.* **2017**, *7*, 5362–5371.
- (9) Herrera-Barros, A.; Bitar-Castro, N.; Villabona-Ortiz, Á.; Tejada-Tovar, C.; González-Delgado, Á. D. Nickel Adsorption from Aqueous Solution Using Lemon Peel Biomass Chemically Modified with TiO₂ Nanoparticles. *Sustainable Chem. Pharm.* **2020**, *17*, 100299.
- (10) Supreetha, R.; Bindya, S.; Deepika, P.; Vinusha, H. M.; Hema, B. P. Characterization and Biological Activities of Synthesized Citrus Pectin-MgO Nanocomposite. *Results Chem.* **2021**, *3*, 100156.
- (11) Ngamsurach, P.; Namwongsa, N.; Praipipat, P. Synthesis of Powdered and Beaded Chitosan Materials Modified with ZnO for Removing Lead (II) Ions. *Sci. Rep.* **2022**, *12*, 17184.
- (12) Shokry Hassan, H.; Elkady, M. F.; El-Shazly, A. H.; Bamufleh, H. S. Formulation of Synthesized Zinc Oxide Nanopowder into Hybrid Beads for Dye Separation. *J. Nanomater.* **2014**, *2014*, 967492.
- (13) Kaur, Y.; Jasrotia, T.; Kumar, R.; Chaudhary, G. R.; Chaudhary, S. Adsorptive Removal of Eriochrome Black T (EBT) Dye by Using Surface Active Low Cost Zinc Oxide Nanoparticles: A Comparative Overview. *Chemosphere* **2021**, *278*, 130366.
- (14) Oyewo, O. A.; Elemike, E. E.; Onwudiwe, D. C.; Onyango, M. S. Metal Oxide-Cellulose Nanocomposites for the Removal of Toxic Metals and Dyes from Wastewater. *Int. J. Biol. Macromol.* **2020**, *164*, 2477–2496.
- (15) Li, C.; Wang, X.; Meng, D.; Zhou, L. Facile Synthesis of Low-Cost Magnetic Biosorbent from Peach Gum Polysaccharide for Selective and Efficient Removal of Cationic Dyes. *Int. J. Biol. Macromol.* **2018**, *107*, 1871–1878.

- (16) Lakouraj, M. M.; Mojerlou, F.; Zare, E. N. Nanogel and Superparamagnetic Nanocomposite Based on Sodium Alginate for Sorption of Heavy Metal Ions. *Carbohydr. Polym.* **2014**, *106*, 34–41.
- (17) Li, Y.; Lv, Z.; Zhang, S.; Zhang, Y.; Wu, S.; Liu, R. Controlled Fabrication and Characterization of α -FeOOH Nanorods. *J. Inorg. Organomet. Polym. Mater.* **2022**, *32*, 1400–1408.
- (18) Dinesh, V. P.; Biji, P.; Ashok, A.; Dhara, S. K.; Kamruddin, M.; Tyagi, A. K.; Raj, B. Plasmon-Mediated, Highly Enhanced Photocatalytic Degradation of Industrial Textile Dyes Using Hybrid ZnO@Ag Core-Shell Nanorods. *RSC Adv.* **2014**, *4*, 58930–58940.
- (19) Aichour, A.; Zaghouane-Boudiaf, H. Highly Brilliant Green Removal from Wastewater by Mesoporous Adsorbents: Kinetics, Thermodynamics and Equilibrium Isotherm Studies. *Microchem. J.* **2019**, *146*, 1255–1262.
- (20) Ibrahim, H. M.; Hamed, A. A. M. Some Physicochemical and Functional Properties of Lemon and Orange Peels. *Int. J. Curr. Microbiol. Appl. Sci.* **2018**, *7*, 4871–4885.
- (21) Šabanović, E.; Memić, M.; Sulejmanović, J.; Selović, A. Simultaneous Adsorption of Heavy Metals from Water by Novel Lemon-Peel Based Biomaterial. *Pol. J. Chem. Technol.* **2020**, *22*, 46–53.
- (22) Abd El-Monaem, E. M.; Monaem, E.; Omer, A. M.; El, G. M.; Mohamed, S.; Eldin, S. M.; Eltaweil, A. S. Zero - Valent Iron Supported - Lemon Derived Biochar for Ultra - Fast Adsorption of Methylene Blue. *Biomass Convers. Biorefin.* **2022**, DOI: 10.1007/s13399-022-02362-y.
- (23) Ibrahim, S. M.; Naghmash, M. A.; El-Molla, S. A. Synthesis and Application of Nano-Hematite on the Removal of Carcinogenic Textile Remazol Red Dye from Aqueous Solution. *Desalin. Water Treat.* **2020**, *180*, 370–386.
- (24) Praipipat, P.; Ngamsurach, P.; Saekrathok, C.; Phomtai, S. Chicken and Duck Eggshell Beads Modified with Iron (III) Oxide-Hydroxide and Zinc Oxide for Reactive Blue 4 Dye Removal. *Arabian J. Chem.* **2022**, *15*, 104291.
- (25) Anushree, C.; Philip, J. Efficient Removal of Methylene Blue Dye Using Cellulose Capped Fe₃O₄ Nanofluids Prepared Using Oxidation-Precipitation Method. *Colloids Surf., A* **2019**, *567*, 193–204.
- (26) Anushree, C.; Nanda Gopala Krishna, D. N. G.; Philip, J. Efficient Dye Degradation via Catalytic Persulfate Activation Using Iron Oxide-Manganese Oxide Core-Shell Particle Doped with Transition Metal Ions. *J. Mol. Liq.* **2021**, *337*, 116429.
- (27) Noreen, S.; Ismail, S.; Ibrahim, S. M.; Kusuma, H. S.; Nazir, A.; Yaseen, M.; Khan, M. I.; Iqbal, M. ZnO, CuO and Fe₂O₃ Green Synthesis for the Adsorptive Removal of Direct Golden Yellow Dye Adsorption: Kinetics, Equilibrium and Thermodynamics Studies. *Z. Physiol. Chem.* **2021**, *235*, 1055–1075.
- (28) Ngamsurach, P.; Praipipat, P. Modified Alginate Beads with Ethanol Extraction of *Cratogeomys formosum* and *Polygonum odoratum* for Antibacterial Activities. *ACS Omega* **2021**, *6*, 32215–32230.
- (29) Threepanich, A.; Praipipat, P. Efficacy Study of Recycling Materials by Lemon Peels as Novel Lead Adsorbents with Comparing of Material Form Effects and Possibility of Continuous Flow Experiment. *Environ. Sci. Pollut. Res.* **2022**, *29*, 46077–46090.
- (30) Ngamsurach, P.; Praipipat, P. Antibacterial Activities against *Staphylococcus aureus* and *Escherichia coli* of Extracted *Piper Betle* Leaf Materials by Disc Diffusion Assay and Batch Experiments. *RSC Adv.* **2022**, *12*, 26435–26454.
- (31) Threepanich, A.; Praipipat, P. Powdered and Beaded Lemon Peels-Doped Iron (III) Oxide-Hydroxide Materials for Lead Removal Applications: Synthesis, Characterizations, and Lead Adsorption Studies. *J. Environ. Chem. Eng.* **2021**, *9*, 106007.
- (32) Langmuir, I. The Adsorption of Gases on Plane Surfaces of Glass, Mica and Platinum. *J. Am. Chem. Soc.* **1918**, *40*, 1361–1403.
- (33) Freundlich, H. M. F. Over the Adsorption in Solution. *J. Phys. Chem.* **1906**, *57*, 385–470.
- (34) Tempkin, M. I.; Pyzhev, V. Kinetics of Ammonia Synthesis on Promoted Iron Catalysts. *Acta Physicochim. URSS* **1940**, *12*, 217.
- (35) Dubinin, M. M.; Radushkevich, L. V. The Equation of the Characteristic Curve of Activated Charcoal. *Proc. USSR Acad. Sci.* **1947**, *55*, 331.
- (36) Jangporn, S.; Youngme, S.; Praipipat, P. Comparative Lead Adsorptions in Synthetic Wastewater by Synthesized Zeolite A of Recycled Industrial Wastes from Sugar Factory and Power Plant. *Heliyon* **2022**, *8*, No. e09323.
- (37) Lagergren, S. About the Theory of So-Called Adsorption of Soluble Substances. *K. Sven. Vetenskapsakad. Handl.* **1898**, *24*, 1–39.
- (38) Ho, Y. S.; McKay, G. Pseudo-Second Order Model for Sorption Processes. *Process Biochem.* **1999**, *34*, 451–465.
- (39) Elovich, S. Y.; Larinov, O. G. Theory of Adsorption from Solutions of Non Electrolytes on Solid (I) Equation Adsorption from Solutions and the Analysis of Its Simplest Form,(II) Verification of the Equation of Adsorption Isotherm from Solutions. *Izv. Akad. Nauk SSSR, Otd. Khim. Nauk* **1962**, *2*, 209–216.
- (40) Weber, W. J.; Morris, J. C. Kinetics of Adsorption Carbon from Solution. *J. Sanit. Eng. Div.* **1963**, *89*, 31–59.